

# Rotating bi-electron in two-dimensional systems with mexican-hat single-electron energy dispersion

V.A. Kochelap

Department of Theoretical Physics, V. Lashkaryov Institute of Semiconductor Physics, NAS of Ukraine, 41, prosp. Nauky, 03680 Kyiv, Ukraine; e-mail: kochelap@ukr.net

**Abstract.** A number of novel two-dimensional materials and nanostructures demonstrate complex single-electron energy dispersion, which is called the *mexican-hat* dispersion. In this paper, we analyze interaction of a pair of electrons with such an energy dispersion. We show that relative motion of the electron pair is of a very peculiar character. For example, the real space trajectories corresponding to electron-electron scattering can have three reversal points, reversal points at non-zero radial momentum and other unusual features. Despite the repulsive Coulomb interaction, two electrons can be coupled forming a composite quasi-particle – the *bi-electron*. The bi-electron corresponds to excited states of the two-electron system. Because the bi-electron coupled states exist in continuum of extended (free) states of the electron pair, these states are quasi-resonant and have finite times of life. We found that rotating bi-electron is a long-living composite quasi-particle. The rotating bi-electrons can be in motion. For slowly moving bi-electrons, we have determined the kinetic energy and the effective mass. Due to strongly nonparabolic energy dispersion, the translational motion of the bi-electron is coupled to its internal motion. This results in effective masses dependent on quantum states of the bi-electron. In the paper, properties of the bi-electron have been illustrated for the example of bigraphene in a transverse electric field.

We have suggested that investigation of rotating bi-electrons at the mexican-hat single-electron energy dispersion may bring new interesting effects in low-dimensional and low-temperature physics.

**Keywords:** bi-electron, energy dispersion, bigraphene.

<https://doi.org/10.15407/spqeo25.03.240>

PACS 73.21.-b

Manuscript received 02.09.22; revised version received 21.09.22; accepted for publication 21.09.22; published online 06.10.22.

## 1. Introduction

It is well known that the crystalline potential affects motion of band electrons (holes) strongly modifying their kinetic energy  $\epsilon(\mathbf{p})$ , where  $\mathbf{p}$  is the electron (hole) momentum. Typically, near an extremum,  $\epsilon(\mathbf{p})$  is of a parabolic dependence with an effective (generally anisotropic) mass. For larger  $\mathbf{p}$ , the nonparabolicity is essential and a portion of the  $\epsilon(\mathbf{p})$  dependence with a negative effective mass ( $d^2\epsilon(\mathbf{p})/dp^2 < 0$ ) can exist. Graphene – atomically thin layer of the carbon atoms – provides the example of striking kinetic energy modification of both electrons and holes, when the  $\epsilon(\mathbf{p})$ -dependences have the linear quasi-relativistic behavior. The bilayer graphene – bigraphene – represents even more complex behavior of low energy  $\epsilon(\mathbf{p})$ -dependences, which additionally can be controlled by external fields. Recently, a few novel materials and nanostructures have been fabricated for which, in the lower energy bands, the

two-dimensional electrons are characterized by complex  $\epsilon(\mathbf{p})$ -dependences that can be called the "mexican-hat" (MH) energy dispersion. For the MH energy dispersion, a local *maximum* occurs say at  $\mathbf{p} = 0$  and a portion with the negative effective mass exists near this maximum. A *minimum* value of  $\epsilon(\mathbf{p})$  is reached at the circle  $|\mathbf{p}| = p_m$ , at larger  $\mathbf{p}$  the function  $\epsilon(\mathbf{p})$  increases. The MH energy dispersion is sketched in Fig. 1a. Examples of two-dimensional materials and nanostructures with this type of the energy dispersion include: bigraphene in a transverse electric field (both, electron and hole bands) [1, 2], hole bands in few-layers III-VI materials, such as GaSe, GaS, InSe, InS and Bi<sub>2</sub>Te<sub>3</sub>, Bi<sub>2</sub>Se<sub>3</sub> [3–6]. Also, the MH energy dispersion is characteristic for HgTe/HgCdTe quantum wells (the upper hole band) [7, 8], InAs/GaAs double quantum well structures [9], the strained quantum well structures fabricated by III-V compound (the upper hole band), including strained GaAs/AlGaAs and GaN/AlGaN structures, *etc.* These

examples indicate that the single-electron energy dispersion of the MH type is quite general phenomenon, especially for two-dimensional systems.

For materials with the MH energy dispersion, relative motion of the electron pair is very specific. Particularly, a repulsive interaction potential can lead to electron pairing, *i.e.* to formation of a composite quasi-particle – a *bi-electron*.

The term “bi-electron” is known in solid-state physics. It was introduced for the case of coupling of two electrons originated from different energy bands, one of them from the bottom of the lower conduction band and the other from the top of an upper band with negative curvature. So that, the reduced effective mass of the pair can be negative, which can give rise to electron pairing in spite of Coulomb repulsion. In particular, the bi-electron model was applied to explain the inverse hydrogen-like series of optical lines observed in layered BiI<sub>3</sub> crystals [10]. Another example of formation of bi-electrons near the saddle points of the two-particle energy dispersion in strong magnetic fields was analyzed in paper by Rashba and Edelstein [11] (quasi-one-dimensional bi-electrons). In both mentioned examples, coupled electrons were originated from different energy bands, the models of the energy dispersion were restricted to parabolic dependences. Note, in composite structures – semiconductor/metal – bi-electron can be formed due to both image forces and spin-orbit interaction [12].

Recently, investigations of electron-electron interaction in graphene-based two-dimensional systems [13] sparked the interest to the bi-electron problem. Indeed, in the paper [14] quasi-localized states of two electrons were found to be possible. Then, the study presented in paper [15] showed that two-electron states can exist, if the single-electron energy dispersion deviates from the linear Dirac-like spectrum. In the cited paper, two-particle states were found for double-layer graphene structures in the model with additional quadratic momentum term with a negative effective mass. This additional term was derived taking into account the

hopping of electrons between the next-nearest-neighbor atoms. The absolute value of effective mass introduced using this way was found about five times larger than the free electron mass. Being applied to single layer or bilayer graphene structures, this approach led to unreasonably large coupling energy ( $\sim 1$  eV).

However, the same model applied to graphene layers separated by boron nitride with the interlayer Coulomb potential led to the coupling energies of the order of tens meV. Further studies of this subject were focused on electron-electron interaction in topological insulators [16], electron pairing was analyzed in the four-band model assuming a step-like repulsive potential.

In this paper, we revisit problems of interaction of two electrons and bi-electron states formation in two-dimensional systems. We assume that coupling energies of pairing electrons are much lower than the energy separation of considered single-electron band in the MH type from other electron bands. We show that, despite the repulsive Coulomb interaction, the two electrons with the single-electron MH dispersion can be coupled forming the excited states of two-electron system. We found that the rotating bi-electrons are of long-living quasi-particles. The rotating bi-electrons can be in translation motion. For slowly moving bi-electron, we determined the kinetic energy and the effective mass. The presented model that exploits the single-electron energy band facilitates the analysis of other important properties of two-dimensional bi-electrons.

The model under consideration is formulated as follows. We consider two-dimensional electron system, when the electron momentum is  $\mathbf{p} = \{p_x, p_y\}$ . We assume that the  $\epsilon(\mathbf{p})$ -dependence is of the MH type, as illustrated in Fig. 1a. This energy is an isotropic function in the  $\{p_x, p_y\}$ -plane. For this type of  $\epsilon(p)$ -dependence, one can introduce a few characteristic parameters: the inflection point,  $p_i$  ( $d^2\epsilon/dp^2 = 0$  at  $p = p_i$ ); the momentum  $p_m$ , corresponding to the energy minimum ( $d\epsilon/dp = 0$  at  $p = p_m$ ) and the momentum  $p_0$ , corresponding to zero energy ( $\epsilon(p_0) = 0$  at  $p_0 \neq 0$ ), as illustrated in Fig. 1b.

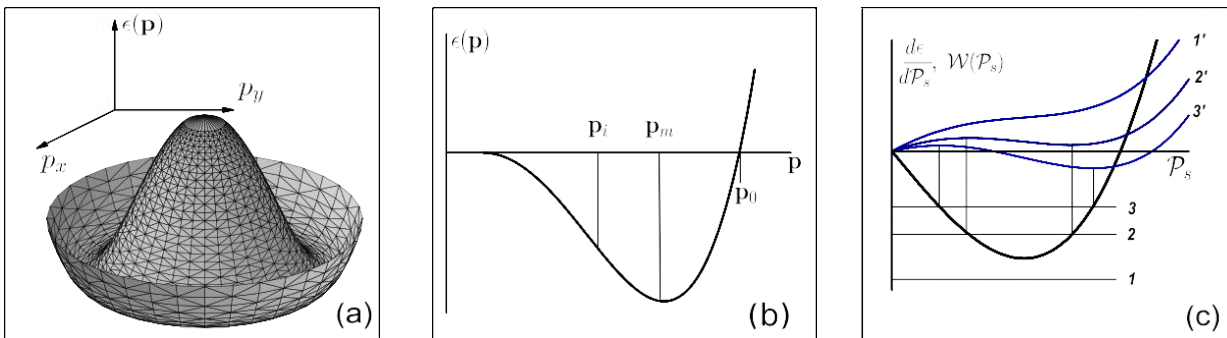


**Fig. 1.** (a) Sketch of the mexican-hat energy dispersion for a two-dimensional quasi-particle. (b) The energy  $\epsilon$  vs the momentum magnitude  $p$ . (c) Illustrations to solutions of Eq. (12) – the l.h.s.,  $d\epsilon/d\mathcal{P}_s$  (the full curve) and the r.h.s.,  $\alpha/p_\phi$  (thin lines) at different  $p_\phi$ ; 1 –  $p_{\phi,1} < p_{\phi,c}$ ; 2 –  $p_{\phi,2} > p_{\phi,c}$ ; 3 –  $p_{\phi,3} > p_{\phi,2}$ . The curves 1', 2', 3' represent the total energy,  $E(\mathcal{P}_s)$ , defined by Eq. (15) for  $p_{\phi,1}$ ,  $p_{\phi,2}$ ,  $p_{\phi,3}$ , respectively. For  $p_\phi = p_{\phi,1}$ , the line 1 does not cross the  $d\epsilon/d\mathcal{P}_s$ -dependence and there are no singular points. For  $p_{\phi,2}$ ,  $p_{\phi,3}$ , intersections of the lines 2, 3 and the  $d\epsilon/d\mathcal{P}_s$ -dependence define the singular points. Thin vertical lines show matching these singular points and extrema of the  $E(\mathcal{P}_s)$ -dependences.

For a pair of the interacting electrons, say 1 and 2, the Hamiltonian is

$$H = \epsilon(\mathbf{p}_1) + \epsilon(\mathbf{p}_2) + U(|\mathbf{r}|), \quad (1)$$

where  $U(|\mathbf{r}|) > 0$  is the potential of the electron-electron interaction, and  $\mathbf{r} = \mathbf{r}_1 - \mathbf{r}_2$  is the relative distance between the electrons. Introducing the total and relative momenta for the two-electron system,  $\mathbf{P} = \mathbf{p}_1 + \mathbf{p}_2$  and  $\mathbf{p} = (\mathbf{p}_1 - \mathbf{p}_2)/2$ , respectively, we rewrite Eq. (1) as  $H = \epsilon(\mathbf{P}/2 + \mathbf{p}) + \epsilon(\mathbf{P}/2 - \mathbf{p}) + U(|\mathbf{r}|)$ . In the absence of external lateral fields in the  $\{x, y\}$ -plane, the total momentum is conserved, *i.e.*,  $\mathbf{P} = \text{constant}$ . Let the center-of-mass for the pair be motionless, *i.e.*,  $\mathbf{P} = 0$ . Then, the Hamiltonian corresponding to relative motion of the two electrons takes the form:

$$H_0 = 2\epsilon(\mathbf{p}) + U(|\mathbf{r}|). \quad (2)$$

This is the basic equation for quantitative analysis given in the following Sections.

Here, we may use Eq. (2) to explain qualitatively two-electron pairing effect at the MH energy dispersion. Indeed, near the point  $\mathbf{p} = 0$  one can simplify  $H_0$  to the form  $H \approx -\mathbf{p}^2/2|M| + U$ , with  $M = 1/(d^2\epsilon(p)/dp|_{p=0})$  being the negative “reduced” effective mass. The auxiliary Hamiltonian,  $H' = -H_0 = \mathbf{p}^2/2|M| - U$ , describes attractive particles that can have coupled states with ‘energies’  $E' < 0$ . Comparing  $H$  and  $H'$ , we can expect that for the Hamiltonian of Eq. (2), coupled states may exist at the energies  $E > 0$ . Since the pairing effect is due to the negative effective mass, radii of coupled states (in real space) have to be sufficiently large to provide (in the momentum representation) the main contribution from small relative momenta  $\mathbf{p}$ , where the negative effective mass occurs. Simultaneously, for the Hamiltonian of Eq. (2), at energies  $E > 0$  there exist also uncoupled states of the electron pair, corresponding to electron-electron scattering. For uncoupled states, the main contribution comes from finite momenta  $\mathbf{p}$  (in the momentum representation). In the semiclassical picture, coupled and uncoupled motions of these two electrons at a given energy are independent: they correspond to different initial conditions. While in the quantum picture, there exists a tunneling between states of the same energy. Therefore, sought-for states have to be *quasi-coupled* and be characterized by a finite decay time. Note, under rotation of the electron pair a finite centrifugal potential gives rise to an increase of the radius of a coupled state, which, in turn, rises its decay time. Concluding this qualitative consideration, one can expect that in the systems with the MH type electron energy it is possible formation of composite quasi-particles – bi-electrons. Bi-electron states are *excited* and metastable states of the two-electron system. The rotating bi-electrons should be long-living quasi-particles.

The rest of the paper is organized as follows. In Section 2, we have presented semiclassical analysis of the problem and give a classification of possible patterns of two-electron motion, and illustrate the results by a few particular models of the MH energy dispersion.

In Section 3, we have developed a quantum approach to the problem, determined energies, wavefunctions, decay times, and spins of these bi-electrons. Finally in this Section, we have considered moving bi-electron. In Section 4, we have discussed the obtained results and presented numerical estimates with focus to the particular example – the bi-layer graphene subjected to a transverse electric field. A short summary of the overall results is presented in Section 5.

## 2. Semiclassical consideration

### 2.1. Equations for relative motion of two electrons

We start with the semiclassical analysis. For such a case, the Hamiltonian of Eq. (2) is a function of two variables, absolute values of the two-dimensional vectors  $\mathbf{p}$  and  $\mathbf{r}$ :  $H_0 = H_0(p, r)$ . It is convenient to use the polar coordinates,  $\{r, \phi\}$ , instead of the orthogonal coordinates,  $\{x, y\}$ , *i.e.*,  $x = r \cos \phi$ ,  $y = r \sin \phi$ . Then, instead of  $p_x$  and  $p_y$  we introduce  $p_r = p_x \cos \phi + p_y \sin \phi$  and  $p_\phi = r(p_y \cos \phi - p_x \sin \phi)$  with  $p^2 = p_r^2 + p_\phi^2/r^2$ . Obviously,  $p_\phi$  is the angular momentum of the pair of electrons. In the new variables,  $\{r, \phi\}$  and  $\{p_r, p_\phi\}$ , Eq. (2) reads

$$H_0(p_r, p_\phi, r, \phi) = 2\epsilon(\sqrt{p_r^2 + p_\phi^2/r^2}) + U(r). \quad (3)$$

The corresponding equations of motion are:

$$\frac{dr}{dt} = \frac{\partial H_0}{\partial p_r} = \frac{2p_r}{\mathcal{P}} \frac{d\epsilon}{d\mathcal{P}} \equiv \mathcal{R}_r(p_r, r|p_\phi), \quad (4)$$

$$\frac{dp_r}{dt} = -\frac{\partial H_0}{\partial r} = \frac{2p_\phi^2}{r^3\mathcal{P}} \frac{d\epsilon}{d\mathcal{P}} - \frac{dU}{dr} \equiv \mathcal{R}_p(p_r, r|p_\phi), \quad (5)$$

$$\frac{d\phi}{dt} = -\frac{\partial H_0}{\partial p_\phi} = \frac{2p_\phi}{r^2\mathcal{P}} \frac{d\epsilon}{d\mathcal{P}}, \quad (6)$$

$$\frac{dp_\phi}{dt} = \frac{\partial H_0}{\partial \phi} = 0. \quad (7)$$

In these equations,  $t$  is the time,  $\frac{d\epsilon}{d\mathcal{P}}$  stands for the derivative of the function  $\epsilon(p)$  calculated at  $p = \mathcal{P} \equiv \sqrt{p_r^2 + p_\phi^2/r^2}$ .

The repulsive potential is supposed to be of the Coulomb type:

$$U(r) = \frac{\alpha}{r}, \quad \alpha > 0, \quad (8)$$

where  $\alpha$  depends on the dielectric environment,  $\mathcal{R}_r$  and  $\mathcal{R}_p$  are designations for the right hand sides of Eqs. (4) and (5), respectively.

The system of Eqs (4)–(7) has the following properties. Eq. (7) implies  $p_\phi = \text{const}$ , which means conservation of the angular momentum. Eqs. (4) and (5) do not depend on the angle  $\phi$ . Thus, the radial motion of the pair described by Eqs (4), (5) and its angular motion described by Eqs (6) and (7) are decoupled. If the radial variables,  $r(t)$  and  $p_r(t)$ , are found, then  $\mathcal{P}$  and  $d\epsilon/d\mathcal{P}$  are known functions of the time,  $t$ , and the angle variable,  $\phi(t)$ , can be easily calculated by using Eq. (6).

## 2.2. Phase-plane analysis

We shall focus on the equations for the radial motion (4), (5), which compose an *autonomous system* of differential equations for the variables  $r$  and  $p_r$ . Such a system can be studied in details by using the so-called phase-plane analysis (see, for example, Ref. [18]). The phase-plane analysis is based on simple reduction of this system to a single differential equation of the first order:

$$\frac{dp_r}{dr} = \frac{\mathcal{R}_p(p_r, r|p_\phi)}{\mathcal{R}_r(p_r, r|p_\phi)}, \quad (9)$$

where the right-hand side (r.h.s.) is parametrically dependent on  $p_\phi$  [19].

At a given  $p_\phi$ , any solution of Eq. (9) can be presented as a certain “trajectory” in the  $\{r, p_r\}$ -phase plane. In these equations,  $t$  is the time,  $dP$  stands for the trajectory corresponds to a certain total energy,  $E$ . The energy conservation law gives the implicit equation of these trajectories,  $H(p_r, r) = E$ . A chosen point in the  $\{r, p_r\}$ -phase plane can be interpreted as an initial condition attributed to a time moment  $t'$ . The trajectory that crosses this point determines the dynamics of the electron pair at  $t > t'$ . By using Eqs (4) and (5), it is easy to determine the direction of the trajectories. The singular points of Eq. (9), if any, correspond to motion of the pair with time-independent  $r$  and  $p_r$  (rotation in real space with a fixed angular velocity according to Eq. (6)). The singular points can be either stable or unstable. Equating the numerator and denominator in Eq. (9) to zero, we obtain two isoclinal lines: a trajectory  $p_r(r)$  crosses the first isoclinal line always horizontally ( $dp_r/dr = 0$ ), while the second isoclinal line is always crossed vertically ( $dp_r/dr = \infty$ ). These properties of the trajectories allow one to reconstruct readily the topology of the phase plane and to study possible types of semiclassical relative motion of the pair of the electrons.

For the singular points ( $r^s, p^s$ ), we obtain the equations

$$p_r^s = 0, \quad (10)$$

$$\frac{2p_\phi}{(r^s)^3} \frac{d\epsilon}{d\mathcal{P}} - \frac{dU}{dr} \Big|_{r^s} = 0 \quad \text{at} \quad \mathcal{P} = \mathcal{P}^s = \frac{p_\phi}{r^s}. \quad (11)$$

For a repulsive potential, we have  $dU/dr < 0$ , thus Eq. (11) may have solutions only at  $d\epsilon/d\mathcal{P} < 0$ . In the case of the energy dispersion shown in Fig. 1b, this leads to the conditions:  $\mathcal{P}^s < p_m$  and  $r^s > p_\phi/p_m$ . Then, using Eq. (8) and the relationship between  $\mathcal{P}^s$  and  $r^s$  we obtain the following simple equation for  $\mathcal{P}^s$ :

$$2 \frac{d\epsilon}{d\mathcal{P}} \Big|_{\mathcal{P}^s} = - \frac{\alpha}{p_\phi}. \quad (12)$$

Here only the left-hand side (l.h.s.) is varied with  $\mathcal{P}^s$ , the r.h.s. is negative and depends parametrically on the angular momentum  $p_\phi$ . For the MH energy dispersion, the l.h.s. is negative at  $\mathcal{P}^s < p_m$  and reaches

a minimum at the inflection point,  $\mathcal{P}^s = p_i$ . Graphical solutions of Eq. (12) are illustrated in Fig. 1c. These solutions arise at

$$p_\phi \geq p_{\phi,c} = \alpha \sqrt{2 \left| \frac{d\epsilon}{d\mathcal{P}} \right|_{p_i}}. \quad (13)$$

At  $p_\phi < p_{\phi,c}$ , Eq. (12) has no solutions and, thus, there are no singular points (see the illustration in Fig. 1c). The corresponding phase portrait of Eq. (9) is shown in Fig. 2a. Trajectories starting and ending at  $r \rightarrow \infty$  correspond to processes of electron-electron scattering and can be called as *scattering trajectories*. Depending on the total energy,  $E$ , there are three types of the scattering trajectories. The type I encloses the trajectories of the energy  $E > E_{c1}$ ,

$$E_{c1} = 2\epsilon(p_m) + \frac{\alpha}{p_\phi} p_m. \quad (14)$$

Each of these trajectories is a continuous line, which starts at  $r \rightarrow \infty$  and  $p_r \rightarrow -p_r(E)$  (with  $p_r(E)$  that satisfies the condition  $2\epsilon(p_r) = E$ ), passes through lower and upper parts of the phase-plane, and finishes with positive  $p_r \rightarrow p_r(E)$  at  $r \rightarrow \infty$ . The trajectory crosses the  $r$ -axis only once at the coordinate  $r = r_E$ , which can be found from the equations:

$$r_E = \frac{p_\phi}{\mathcal{P}_E}, \quad E = 2\epsilon(\mathcal{P}_E) + \frac{\alpha}{p_\phi} \mathcal{P}_E \equiv W(\mathcal{P}_E). \quad (15)$$

For this type of the trajectories,  $W(\mathcal{P}_E)$ -dependence is illustrated in Fig. 1c by the curve  $I'$ . The trajectories have a single *reversal point* ( $r_E, 0$ ) with  $r_E < p_\phi/p_m$ . At the reversal point, the radial velocity changes its sign. The type I of the phase-plane trajectories corresponds to usual processes of elastic scattering in real space.

The type II encloses trajectories of the energy interval  $0 < E < E_{c1}$ . At large  $r$ , they behave similarly to the type I, however, they have unusual feature at finite  $r$ . Indeed, for these trajectories there exist *three reversal points*. For each of these trajectories, one of the reversal point lies on the  $r$ -axis and is determined by Eqs (15). Two other ones are on the line  $p_r = \pm \sqrt{p_m^2 - p_\phi^2/r^2}$ . For a given energy  $E$ , the additional reversal points occur at

$$r_{r,E}^{ad} = \frac{\alpha}{E - 2\epsilon(p_m)}, \quad (16)$$

$$p_{r,E}^{ad} = \pm \sqrt{p_m^2 - \frac{p_\phi^2}{\alpha^2} [E - 2\epsilon(p_m)]^2}.$$

From Eq. (6), it follows that at the additional reversal points, the angular velocity,  $d\phi/dt$ , changes its sign.

The trajectories with  $E < 0$  never cross the  $r$ -axis, they can be attributed to the type III. For this case, there are two solutions of the equation  $2\epsilon(p) = E$ , which we denote  $p^m(E)$  and  $p^M(E)$  with  $p^m < p_m < p^M$ . This implies the existence of two isolated trajectories for a given negative  $E$ . One trajectory starts at infinity ( $r \approx \infty$ ) with

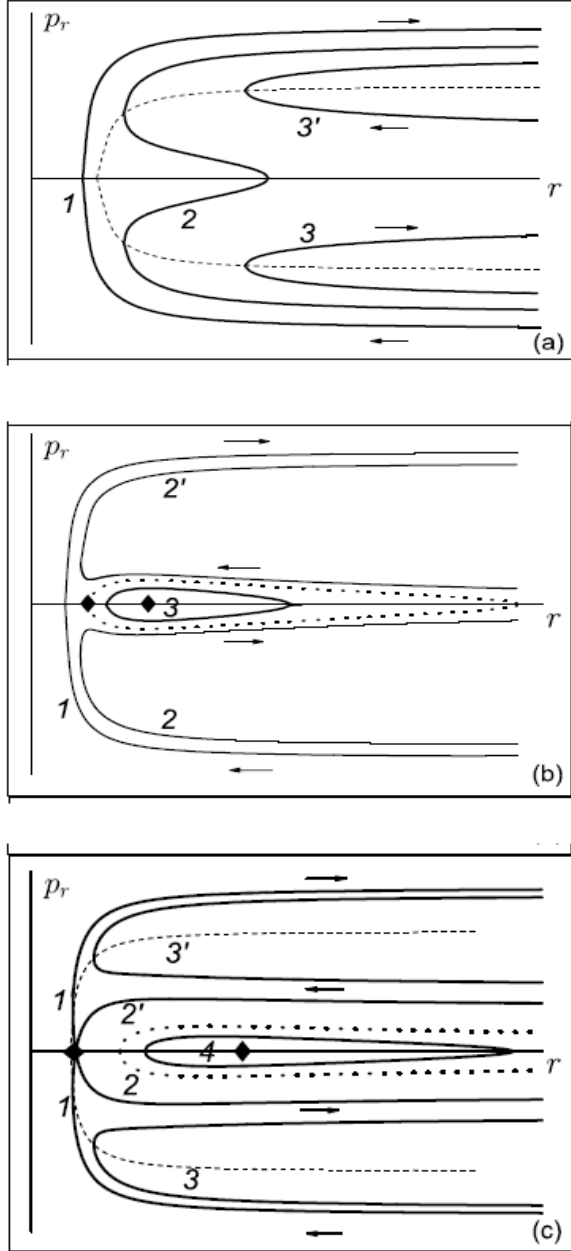


**Fig. 2.** Phase portraits of Eq. (9) at different values of the angular momentum,  $p_\phi$ . Solid lines are trajectories, dashed lines (in (a) and (c)) correspond to the equation  $p^2 + p^2/r^2 = p$ . The arrows indicate direction of motion along the trajectories. (a) The case  $p_\phi < p_{\phi,c}$ ; curves 1, 2 are scattering trajectories of the type I and II, respectively. Trajectories are presented for different values of the total energy,  $E$ : curve 1 for  $E > E_{c1}$ , the type I; curve 2 for  $E_{c1} > E > 0$ , the type II; curves 3, 3' for  $E < 0$ , the type III. (b) The case  $p_\phi > p_{\phi,c}$  and  $E^{s1}, E^{s2} > 0$ ; for two singular points are marked with asterisks. Dotted line is the separatrix closed loop restricting a region of the phase plane with the closed trajectories. Curves 1, 2, 2' are trajectories of the scattering types I and III; curve 3 is an example of the closed trajectories with  $E^{s1} > E > E^{s2}$ . (c) The case  $p_\phi > p_{\phi,c}$  and  $E^{s1} > 0, E^{s2} < 0$ ; curves 1, 2, 2', 3, 3' are trajectories of the scattering types. The dotted line restricts the region with closed trajectories. Curve 4 is an example of the closed trajectory for  $E^{s1} > E > 0$ .

$p_r = -p^M(E)$ . It has a reversal point given by Eq. (16) with its sign in the second equation, remains in the lower part of the  $(r, p_r)$ -plane, and finishes at infinity with  $p_r = -p^M(E)$ . Another one starts at infinity with  $p_r = +p^M(E)$  and finishes at infinity with  $p_r = +p^M(E)$ . Corresponding reversal point is determined by Eq. (16) with its sign. Despite the elastic character of the processes, these trajectories describe collisions that give rise to a change of the relative momentum,  $p_r$ , of the electron pair.

Now, we return to the case when the inequality (13) holds and Eq. (9) has singular points. The single such point ( $r_s = p_\phi/p_i, p_r = 0$ ) appears in the phase-plane at  $p_\phi = p_{\phi,c}$ . When  $p_\phi > p_{\phi,c}$ , Eq. (11) has two solutions  $\mathcal{P}^{s1}$  and  $\mathcal{P}^{s2}$  with  $\mathcal{P}^{s1} < p_i < \mathcal{P}^{s2} < p_m$  (see illustration in Fig. 1c). Thus, there are two singular points ( $r^{s1}, 0$ ) and ( $r^{s2}, 0$ ),  $r^{s1} > r^{s2}$ . Near a singular point ( $r^s, 0$ ), the trajectories corresponding to different energies  $E$  can be found in the form:

$$\frac{1}{\mathcal{P}^s} \frac{d\epsilon}{d\mathcal{P}^s} p_r^2 + \frac{(\mathcal{P}^s)^4}{p_\phi^2} \frac{d^2\epsilon}{d(\mathcal{P}^s)^2} (r - r^2)^2 = E - E^s, \quad (17)$$

where  $E^s$  is the total energy of relative motion of the electron pair in the  $s$ -th singular point defined by the second equation from (15):  $E^s = E(\mathcal{P}^s)$ . For the  $s1$ -point

with  $\frac{d\epsilon}{d\mathcal{P}^s} < 0$  and  $\frac{d^2\epsilon}{d(\mathcal{P}^s)^2} < 0$  (see Fig. 1c), from

Eq. (17), it follows that allowed energies are  $E < E^s$  and the trajectories are closed curves. That is, the  $s1$ -point is the center. While for the  $s2$ -point with  $\frac{d\epsilon}{d\mathcal{P}^s} < 0$  and  $\frac{d^2\epsilon}{d(\mathcal{P}^s)^2} > 0$ , the trajectories are hyperboles.

This  $s2$ -point is the saddle one. The appearance of the singular points leads to restructuring of the phase-plane. There can exist two cases of different phase-plane topologies.

For the first case, the phase-plane is presented in Fig. 2b. For this case, both singular points correspond to positive total energies,  $E^{s1}, E^{s2} > 0$ , defined by Eq. (15) at  $\mathcal{P}_E = \mathcal{P}^{s1}, \mathcal{P}^{s2}$ , as illustrated by the curve 2' in Fig. 1c. In the phase-plane in Fig. 2b, two separatrices of the saddle form a closed loop that restricts a finite region of the phase-plane, where all the trajectories are closed. For them, the total energy  $E$  is in the range  $E^{s1} > E > E^{s2} > 0$ . For a given energy from this range, the minimal and maximal coordinates,  $r_m(E)$  and  $r_M(E)$ , which can be reached on the closed trajectory, are to be found from Eq. (15). Note, for the same energy range there are trajectories of a scattering type. The latter are well separated from the closed ones, as illustrated in Fig. 2b by curves 1, 3. Outside the discussed energy range, all the trajectories are of the scattering types, as was found in the previous analysis.

Another case of the phase-plane topology is shown in Fig. 2c. It occurs for  $E^{s1} > 0 > E^{s2}$ , as illustrated by the curve 3' in Fig. 1c. For other fixed parameters, this case

corresponds to larger angular momenta. Now the separatrices of the  $s_2$ -saddle are extended up to infinity; they do not form any closed loop. Instead, the closed trajectories exist for the energy interval  $E^{s_1} \geq E > 0$ . For  $E \rightarrow +0$ , these closed trajectories are extended to infinitely large  $r$ . With increase in  $p_\phi$ , the singular points move toward larger  $r$ . At  $p_\phi \gg \frac{\alpha}{2p_i \left| \frac{d^2\epsilon}{dp^2} \right|_{p=0}}$  one can

obtain  $r^{s_1} \approx 2 \left| \frac{d^2\epsilon}{dp^2} \right|_{p=0} \frac{p_\phi^2}{\alpha} \propto p_\phi^2$  and  $r^{s_2} \approx \frac{p_\phi}{p_0} \propto p_\phi$ . The

region of the phase-plane, which contains the closed trajectories, also is shifted toward larger  $r$ . Under discussed strong inequality, the Hamiltonian of Eq. (3) is simplified to the form

$$H_0 = - \left| \frac{d^2\epsilon}{dp^2} \right|_{p=0} \left( p_r^2 + \frac{p_\phi^2}{r^2} \right) + \frac{\alpha}{r}. \quad (18)$$

Following the discussion presented in Introduction, one can introduce the auxiliary Hamiltonian  $H'_0 = -H_0$ , that can be easily reduced to that of the well known Kepler problem. Detailed analysis of this problem can be found elsewhere [20]. Particularly, from this analysis, it follows that the closed trajectories exist for the energy interval  $0 < E < E^{s_1} = \alpha/4p_\phi^2 \left| d^2/dp^2 \right|_{p=0}$ .

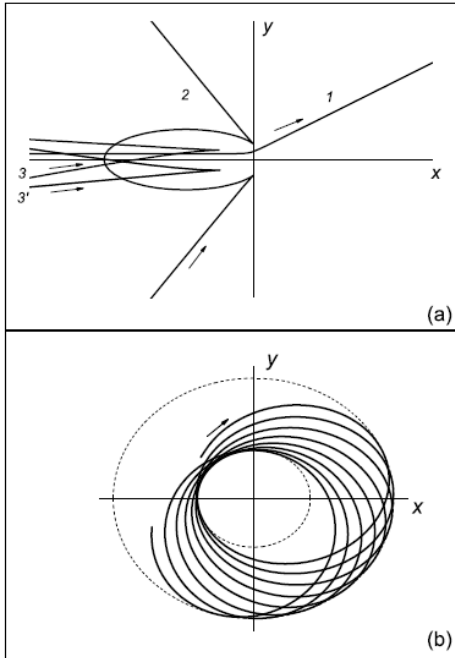


**Fig. 3.** Trajectories in real space. (a) Scattering trajectories; curves 1, 2 and 3, 3' are scattering trajectories of the types I, II, and III, respectively; they correspond to the phase-plane trajectories 1, 2 and 3, 3' shown in Fig. 2a. (b) A real-space trajectory illustrating bounded motion of the electron pair. Dashed circles mark the minimal and maximal distances between electrons.

Now consider briefly relative motion of the pair of the electrons in *real space*. Trajectories in the  $\{x, y\}$ -real space can be calculated, when solutions of Eqs (4) and (5), for  $r(t)$  and  $\phi(t)$ , are found. Examples of the scattering trajectories are shown in Fig. 3a. Among the presented curves, only trajectory 1 has a standard form for the process of scattering by a repulsive potential. Shapes of the others are rather unusual, which is caused by the complex energy dispersion of the MH type. For example, the curve 2 represents scattering trajectory with three reversal points, the curves 3, 3' represent trajectories with single reversal points occurring at a finite radial momentum (matching these real-space trajectories to those of the phase-plane is indicated in the caption). Note, among trajectories belonging to the type II there are self-crossing trajectories in real space (not shown in Fig. 3a).

The closed trajectories in the  $\{r, p_r\}$ -phase-plane correspond to relative motion of two electrons, which occurs in a restricted region of real space. At a given energy  $E$ , the real space trajectory lies in a ring bounded by the circles of radii  $r_m(E)$  and  $r_M(E)$ , both were defined above. Generally, these trajectories are not closed, as illustrated in Fig. 3b. At a given angular momentum  $p_\phi$ , the only closed real-space trajectory is a circular orbit with the radius corresponding to the  $s_1$  singular point:  $r = r^{s_1}$  at  $E = E^{s_1}$ . The electron pair moves round this orbit with the velocity  $2 \left| d^2\epsilon/dp^2 \right|_{p=p_\phi/r^{s_1}}$ . The corresponding

rotation frequency is  $\Omega^{s_1} = 2 \left/ \left( r^{s_1} \left| d^2\epsilon/dp^2 \right|_{p=p_\phi/r^{s_1}} \right) \right| d^2\epsilon/dp^2 \Big|_{p=p_\phi/r^{s_1}}$ . For motion with the energy  $E$  close to  $E^{s_1}$ , the rotation occurs with small radial vibrations. The frequency and magnitude of these vibrations are equal to

$$\Omega_r = \frac{2p_\phi^{1/2}}{r^{s_1 3/2}} \sqrt{\frac{d\epsilon}{dp} \frac{d^2\epsilon}{dp^2}},$$

$$r_M - r_m = 2 \frac{r_{s_1}^2}{p_\phi} \sqrt{\frac{E^{s_1} - E}{\left| d^2\epsilon/dp^2 \right|}}, \quad (19)$$

where  $E < E^{s_1}$  and the derivatives are calculated at  $p = p_\phi/r^{s_1}$ . Obviously, spatially bounded relative motion of the two electrons means their coupling despite repulsive interaction.

Summarizing, the general analysis showed that the two-electron coupling in real space arises with the onset of the singular points,  $s_1, s_2$ , in the  $\{r, p_r\}$  phase-plane of Eq (9). Eqs (10), (11) and (15) for these points facilitate the determination of the energies of  $E^{s_1}, E^{s_2}$ , corresponding to these points at a given angular momentum,  $p$ . The two-electron coupling is realized for the following interval of the total energy:  $\max\{0, E^{s_2}\} < E < E^{s_1}$ .

### 2.3. Numerical estimates

It is useful to conclude the semiclassical analysis with numerical estimates. We rescale the variables as follows:

$$\mathbf{k} = \frac{\mathbf{p}}{p_B}, \quad l_\phi = \frac{p_\phi}{l_{\phi,B}}, \quad \boldsymbol{\rho} = \frac{\mathbf{r}}{r_B}, \quad \varepsilon(\mathbf{k}) = 2 \frac{\varepsilon(\mathbf{p})}{E_B},$$

$$\mathfrak{K}_0 = \frac{H_0}{E_B} = \varepsilon(\mathbf{k}) + \frac{1}{\rho}, \quad (20)$$

where we introduce the Bohr-like units:

$$p_B = \frac{M\alpha}{\hbar}, \quad r_B = \frac{\hbar}{p_B}, \quad E_B = \frac{M\alpha^2}{\hbar^2}, \quad M = \frac{1}{2|d^2\varepsilon/dp^2|_{p=0}},$$

$$p_{\phi,B} = p_B r_B = \hbar.$$

Here,  $M$  is the reduced mass of the pair at  $p \rightarrow 0$ . In the dimensionless form, Eqs (15) that define the singular points are:

$$\rho_\varepsilon = l_\phi / \mathfrak{K}_\varepsilon, \quad \varepsilon = \varepsilon(\mathfrak{K}_\varepsilon) + \mathfrak{K}_\varepsilon l_\phi / l_\phi \equiv \mathfrak{W}(\mathfrak{K}_\varepsilon), \quad (21)$$

where  $\mathfrak{W}(\mathfrak{K})$  and  $\mathfrak{K}_\varepsilon$  are the dimensionless analogs of  $W(\mathcal{P})$  and  $\mathcal{P}_E$  defined by Eqs (15). Bellow,  $\varepsilon$  presents the dimensionless total energy of the pair. This formal scaling to the Bohr units will allow us to compare the results with those known from the quantum Coulomb problem.

As the first example, we consider the simplest model of the MH type energy dispersion, for which the dimensionless kinetic energy of relative motion of the electron pair is

$$\varepsilon(k) = -\frac{1}{2}k^2 + \beta k^4, \quad \beta > 0. \quad (22)$$

The corresponding characteristic parameters (see Fig. 1b) are:  $k_i = 1/2\sqrt{3\beta}$ ,  $k_0 = 1/\sqrt{2\beta}$ ,  $k_m = 1/2\sqrt{\beta}$ ,  $\varepsilon(k_m) = 1/16\beta$ . According to Eq. (13), the critical angular momentum necessary for the existence of the singular points and the closed trajectories equals  $l_\phi = l_{\phi,c} = 3\sqrt{3\beta}$ . For this  $l_\phi$ , the singular point in the  $\{\rho, k_\rho\}$  phase-plane arises at  $k_{\rho,s} = 0$ ,  $\rho_{s,c} = 2\sqrt{3\beta}$  ( $\varepsilon_{s,c} = \mathfrak{W}(k_i) = 1/48\beta$ ).

If we assume  $\beta = 0.25$ , then we obtain:  $k_i = 0.58$ ,  $k_m = 1$ ,  $k_0 = 1.41$ ,  $\varepsilon(k_m) = -0.25$ ,  $l_{\phi,c} = 2.6$ , the energy corresponding to the onset of the singular points is  $\varepsilon_{s,c} = 0.08$ , and the radius of the emerging circular orbit is  $\rho_{s,c} \approx 7.6$ . Setting  $l_\phi = 3$ , we found that the closed trajectories occur in a finite energy interval,  $0.05 < \varepsilon < 0.06$ . In real space, all the closed trajectories are located within the ring  $4 \leq \rho \leq 7.5$ . Setting  $\beta = 0.5$ , we found  $k_i = 0.41$ ,  $k_m = 0.7$ ,  $\varepsilon(k_m) = -0.125$ ,  $l_{\phi,c} = 3.67$ ,  $\varepsilon_{s,c} = 0.04$  and  $\rho_{s,c} = 9$ . Assuming  $l_\phi = 4$ , we found for the closed trajectories  $0.031 \leq \varepsilon \leq 0.034$  and  $8 \leq \rho \leq 13$ . At  $l_\phi = 5$ , for the same characteristics we found  $0 \leq \varepsilon \leq 0.02$  and  $8.8 \leq \rho \leq 22$  for the closed trajectories.

These estimates illustrate that, increasing  $\beta$  and shortening the negative effective mass, the portion of  $\varepsilon(k)$  leads to larger critical values of the angular momentum,  $l_{\phi,c}$ , greater sizes of the coupled electron pair and lower its energies of coupling.

As a second example of the energy dispersion of MH type, we consider the lowest electron (or hole) band of bigraphene subjected to a voltage applied across the graphene layers. For this case, the one-particle energy is [1]:

$$\varepsilon(p) = \sqrt{g^2/2 + V^2/4 + p^2 v_F^2 - \sqrt{g^4/4 + p^2 v_F^2 (g^2 + V^2)}}, \quad (23)$$

here,  $v_F$  is the Fermi-velocity parameter of graphene,  $g$  ( $\approx 0.4$  eV) characterizes interaction between graphene layers, and  $V$  is the voltage bias applied across the layers. Assuming bigraphene on a substrate with a dielectric constant  $\kappa_0$ , for the Coulomb potential (8) we obtain  $\alpha = 2e_0^2/(1 + \kappa_0)$  with  $e_0$  being the elementary charge. Next, we introduce the scaling parameters as in Eqs (20)

$$p_B = \frac{e_0^2 g^2}{2\hbar v_F^2 V(1 + \kappa_0)}, \quad r_B = \frac{2\hbar^2 v_F^2 V(1 + \kappa_0)}{e_0^2 g^2},$$

$$E_B = \frac{e_0^4 g^2}{2\hbar^2 v_F^2 V(1 + \kappa_0)^2}. \quad (24)$$

The dimensionless two-particle energy  $\varepsilon(k) = 2[\varepsilon(k_{pB}) - \varepsilon(0)]/E_B$  at small  $k$  behaves as  $\varepsilon(k) \approx -k^2/2 + \dots$

For further estimates, we set  $V = 0.25$  eV (corresponding energy gap of bigraphene is about 0.21 eV) and  $\kappa_0 = 3.9$ , the latter is valid for SiO<sub>2</sub> substrate. We find

$$M = 0.028m_0, \quad E_B = 0.128 \text{ eV}, \quad p_B/\hbar = 2.18 \cdot 10^6 \text{ cm}^{-1},$$

$$r_B = 4.58 \cdot 10^{-7} \text{ cm}. \quad (25)$$

Here,  $m_0$  is the free electron mass. The characteristic parameters of the two-particle kinetic energy  $\varepsilon(k)$  are:  $k_i = 0.62$ ,  $k_m = 1.14$ ,  $k_0 = 1.74$ ,  $\varepsilon(k_m) = -0.3$  (i.e.,  $\approx 0.038$  eV). Then, we obtain the critical value of the angular momentum,  $l_{\phi,c} = 2.5$ , the energy corresponding to the onset of the singular points,  $\varepsilon_{s,c} = \mathfrak{W}(k_i) = 0.09$ , and the radius of the emerging circular orbit,  $\rho_s \approx 4.25$ . Setting  $l_\phi = 3$ , we find that the closed trajectories occur in a finite energy interval,  $0.04 < \varepsilon < 0.06$  at  $0.16 < \mathfrak{K}_\varepsilon < 0.83$  (see Eq. (21)). In real space, all the closed trajectories are located within the ring  $3.6 \leq \rho \leq 19$ . Setting  $l_\phi = 4$ , we found that these trajectories occur at  $0 < \varepsilon < 0.03$ ,  $\mathfrak{K}_\varepsilon < 0.6$  and the inter-particle distance  $\rho > 6.6$ .

These estimates show that semiclassical trajectories corresponding to spatially bound relative motion of the two electrons exist only for finite values of the angular momentum  $l_\phi$ . That is, *to be coupled the pair of electrons has to rotate*. The energy of the coupled electrons is always positive and less than  $|\varepsilon(k_m)|$ . Note, for any energy corresponding to a trajectory of coupled motion there always exists a trajectory of uncoupled motion. The trajectories of coupled and uncoupled motion are well separated in the  $\{\rho, k_\rho\}$  phase-space.

### 3. Quantum analysis

Foregoing semiclassical analysis allowed us to understand qualitative features of relative motion of the electron pair with the MH energy dispersion. However, as can be seen from numerical estimates, it shows that this analysis is not always adequate for quantitative conclusions. Below we develop a quantum approach to the problem under consideration.

For the quantum analysis, we assume that spin-orbit interaction is negligible and orbital motion and spin motion can be separated. First, we will focus on the orbital motion.

#### 3.1. Quantum equations for orbital motion of the electron pair

We will use the dimensionless variables of Eq. (20) and, particularly, the Hamiltonian  $\mathfrak{H}_0$  with  $\mathfrak{E}(\hat{\mathbf{k}})$  being the function of the momentum operator  $\hat{\mathbf{k}} = -i \frac{\partial}{\partial \rho}$ . Thus, in the coordinate representation the Schrödinger equation for relative motion of the electron pair is [21]

$$\hat{\mathfrak{H}}_0 \Psi(\rho) = \left[ \mathfrak{E}(\hat{\mathbf{k}}) + \frac{1}{\rho} \right] \Psi(\rho) = \mathfrak{E} \Psi(\rho) \quad (26)$$

Because of the circular symmetry of the problem, we will use the polar coordinates  $\rho, \phi$ , then  $\Psi(\rho) = \Psi(\rho, \phi)$ . The angular momentum operator is  $\hat{l} = -i \frac{\partial}{\partial \phi}$ ; its eigenfunctions and eigenvalues are

$$\Psi_l(\phi) = \frac{1}{\sqrt{2\pi}} e^{-i l \phi}, \quad l = 0, \pm 1, \pm 2, \quad (27)$$

The operator  $\hat{l}$  commutes with  $\mathfrak{H}_0$ , thus we can set

$$\Psi(\rho, \phi) = R_l(\rho) \Phi_l(\phi). \quad (28)$$

Keeping in mind that the semiclassical analysis proves the existence of rotating coupled electron pairs, below we consider solutions to Eq. (26) with  $|l| \geq 1$ .

To obtain equation for the radial functions,  $R_l(\rho)$ , we use the following relationship valid for a two-dimensional system:

$$\begin{aligned} \hat{k}^2 R_l(\rho) \Phi_l(\phi) &\equiv -\Delta_2 R_l(\rho) \Phi_l(\phi) = \\ &= \Phi_l(\phi) \left[ -\frac{1}{\rho} \frac{d}{d\rho} \rho \frac{d}{d\rho} + \frac{l^2}{\rho^2} \right] R_l(\rho), \end{aligned} \quad (29)$$

where  $\Delta_2$  is the two-dimensional Laplacian. Now, from Eq. (26) we can formally write down the operator equation for  $R_l(\rho)$

$$\left[ \mathfrak{E} \left( \sqrt{-\frac{1}{\rho} \frac{d}{d\rho} \rho \frac{d}{d\rho} + \frac{l^2}{\rho^2}} \right) + \frac{1}{\rho} \right] R_l(\rho) = \mathfrak{E}_l R_l(\rho), \quad (30)$$

where generally dependent on  $l$  eigenvalue,  $\mathfrak{E}_l$ , is introduced.

To solve the operator equation (30), we will use the eigenfunctions of the operator  $\left[ -\frac{1}{\rho} \frac{d}{d\rho} \rho \frac{d}{d\rho} + \frac{l^2}{\rho^2} \right]$ , which are known to be the Bessel function,  $J_l(q\rho)$ , [22]:

$$\left[ -\frac{1}{\rho} \frac{d}{d\rho} \rho \frac{d}{d\rho} + \frac{l^2}{\rho^2} \right] J_l(q\rho) = q^2 J_l(q\rho). \quad (31)$$

Note, for arbitrary operator of the kinetic energy  $\mathfrak{E}(\hat{\mathbf{k}})$ , the radial function of free particles with an energy  $\mathfrak{E}$  can be also expressed via the Bessel function:

$$\mathfrak{R}_{l,\mathfrak{E}}(\rho) = J_l(q_{\mathfrak{E}}\rho), \quad (32)$$

where  $q_{\mathfrak{E}}$  solves the equation  $\mathfrak{E}(q_{\mathfrak{E}}) = \mathfrak{E}$ .

Below we will use *Fourier–Hankel transformation* [23]:

$$R_l(q) = \int_0^{\infty} d\rho \rho R_l(\rho) J_l(q\rho). \quad (33)$$

It is important that, for functions in the form of Eqs (27) and (28) with integer  $l$ , standard two-dimensional *Fourier transformation* between real space and momentum space,

$$\Psi(\rho) = \frac{1}{2\pi} \int d^2 q \Phi(q), \quad \Phi(q) = \frac{1}{2\pi} \int d^2 \rho \Psi(\rho),$$

also leads to the relation (33) for the radial functions  $\mathfrak{R}_l(\rho)$  and  $\mathfrak{R}_l(q)$ . In particular, this is valid for solutions of the well known two-dimensional Coulomb problem with attractive potential,  $\mathfrak{R}_l(\rho)$  and  $\mathfrak{R}_l(q)$  (see, for example, Ref. [24]).

Now we transform Eq. (30) to the integral equation

$$[\mathfrak{E}(q) - \mathfrak{E}_l] R_l(q) + \int_0^{\infty} dq' Q_l(q, q') R_l(q') = 0, \quad (34)$$

with the symmetrical kernel

$$Q_l(q', q) = \int_0^{\infty} d\rho J_l(q'\rho) J_l(q\rho). \quad (35)$$

For  $q' > q$ , the kernel explicit form is [22]:

$$\begin{aligned} Q_l(q', q) &= \frac{\Gamma\left(l + \frac{1}{2}\right)}{\sqrt{\pi}(\Gamma(1+l))} (q')^{-1-l} q^l \times \\ &\times {}_2F_1\left(\left[\frac{1}{2}, l + \frac{1}{2}\right], [1+l], \frac{q^2}{(q')^2}\right). \end{aligned} \quad (36)$$

Here,  $\Gamma(x)$  and  ${}_2F_1([a, b], c, x)$  are the gamma and hypergeometric functions, respectively. For  $q' < q$ , the kernel can be obtained from Eq. (36) by permutation

$q' \leftrightarrow q$ . This permutation recovers the symmetry property of the kernel  $Q_l(q', q)$ .

Eq. (34) is the equation for the radial function in momentum space. It is important that in Eq. (34)  $\varepsilon(q)$  is the usual function, which according to scaling (20) at small  $q$  behaves as  $\varepsilon(q) \approx -\frac{1}{2}q^2 + \dots$ .

### 3.2. Approximate solutions for the wavefunctions

According to the above semiclassical analysis, in the same energy interval, where closed trajectories (in the phase-plane) of the electron pair occur, there also exist trajectories of the uncoupled motion. Thus, in the quantum analysis, we can expect a *quasi-resonant character* of coupled states of the electron pair. We will seek for solutions to Eq. (34) in the form

$$R_l(q) = \sum_n B_n^l \bar{R}_{l,n}(q) + \mathfrak{B}_l, \quad (37)$$

where  $\{\bar{R}_{l,n}(q)\}$  is a set of given functions describing localized states.  $\mathfrak{B}_l$  is a small contribution of unbound (free) states of the pair, it will be analyzed in the following subsection.

As a set of functions  $\{\bar{R}_{l,n}\}$ , we select the solutions of the two-dimensional Coulomb problem with the attractive potential. For the momentum representation, detailed analysis of this problem has been done in the papers [24]. Corresponding functions are solutions for the equation

$$\left[ \frac{1}{2}q^2 - \bar{\varepsilon}_n \right] \bar{R}_{l,n}(q) - \int_0^\infty dq' Q_l(q, q') \bar{R}_{l,n}(q') = 0, \quad (38)$$

with  $\bar{\varepsilon}_n = -1/2(n+1/2)^2$  valid at  $n \geq |l|$ , i.e., a given  $n^{\text{th}}$ -state of the two-dimensional Coulomb problem is  $(2n+1)$ -fold degenerated. The explicit expressions of normalized functions  $\bar{R}_{l,n}(q)$  are

$$\begin{aligned} \bar{R}_{l,n}(q) = & (-1)^l i^n 2 \sqrt{(2n+1)} \frac{(n-|l|)!}{(n+|l|)!} \times \\ & \times \frac{q_n^2}{(q_n^2 + q^2)^{3/2}} \mathfrak{P}_n^l \left[ \frac{q_n^2 - q^2}{q_n^2 + q^2} \right], \end{aligned} \quad (39)$$

where  $\mathfrak{P}_n^l[x]$  is associated Legendre polynomials,  $q_n = 1/(n+1/2)$ . One can show that, in momentum space these wavefunctions are essentially concentrated within the range of small momenta,  $q \leq 1/(n+1/2)$ . The degree of localization of the functions in small  $q$ -range increases for larger  $l$  and  $n$ .

Return to solutions of Eq. (34) in the form (37). Multiplying Eq. (38) by  $-1$  and comparing it with Eq. (34), we can see that for  $\bar{\varepsilon}_l > 0$  both equations are quite similar, the only difference is more complex dependence of  $\varepsilon(q)$ . Accordingly, for the coefficients  $B_n^l$  we obtain the following equations:

$$[\bar{\varepsilon}_l - |\bar{\varepsilon}_{l,n}|] B_n^l - \sum_{n' \geq l} \langle \bar{R}_{l,n}^* | E(q) + \frac{1}{2}q^2 | \bar{R}_{l,n'} \rangle B_{n'}^l = 0, \quad (40)$$

where  $n > l$  and  $\langle \bar{R}_{l,n}^* | \dots | \bar{R}_{l,n'} \rangle$  mean the matrix element calculated on the Coulomb states  $\{l, n\}$  and  $\{l, n'\}$ . In this formulation, the difference of eigenvalues for the considered problem from the Coulomb ones is expressed *via* deviation of  $\varepsilon(q)$  from the parabolic law.

Eqs (40) can be solved numerically for a given  $\varepsilon(q)$  dependence. Below we present results obtained for  $\varepsilon(q)$  corresponding to Eq. (23) at parameters discussed in Section 2 (bigraphene on SiO<sub>2</sub> substrate). The procedure of solution of Eq. (40) is the following (Galerkin) method. We use a finite number of the functions,  $\{\bar{R}_{l,l}, \bar{R}_{l,l+1}, \dots, \bar{R}_{l,l+v-1}\}$ . This gives us  $v$  approximate eigenvalues designated as  $\varepsilon_{l,N}^{(v)}$ ,  $N = l, l+1, l+2, \dots, l+v-1$  and corresponding eigenvectors  $\{B_N^{l,(v)}\}$ . Then, we increase the integer  $v$  until we reach the discrepancy  $|\varepsilon_{l,N}^{(v)} - \varepsilon_{l,N}^{(v+1)}| / \varepsilon_{l,N}^{(v)} < 0.001$ , for four lower states with  $N = l, \dots, l+3$ . The obtained values  $\varepsilon_{l,N}$  are presented in Table. There, for comparison we also show four eigenvalues,  $|\varepsilon_{N,\text{Coul}}|$ , of the two-dimensional Coulomb problem of Eq. (38).

Similarly to the Coulomb problem, one can consider  $N$  as the “main quantum number”. However, unlike the Coulomb problem we obtain an *inverse series* of the energy levels: all quasi-bound states are excited states, and larger main quantum number  $N$  corresponds to smaller energy  $E_{l,N}$ . From the results of Table, one may

**Table.** Calculated energies,  $\varepsilon_{l,N}$ , broadenings,  $\gamma_{l,N}$ , and total spins,  $\Sigma$ , of different quasi-coupled states for the example of bigraphene on SiO<sub>2</sub> substrate discussed in the text. Energies of the Coulomb states,  $|\varepsilon_{N,\text{Coul}}|$ , are presented for comparison.

$N$	$\varepsilon_{N,\text{Coul}}$	$\varepsilon_{1,N}$	$\gamma_{1,N}$	$\Sigma$	$\varepsilon_{2,N}$	$\gamma_{2,N}$	$\Sigma$	$\varepsilon_{3,N}$	$\gamma_{3,N}$	$\Sigma$	$\varepsilon_{4,N}$	$\gamma_{4,N}$	$\Sigma$
1	0.222	0.337	0.176	1									
2	0.08	0.102	0.028	1	0.094	0.001	0						
3	0.041	0.048	0.007	1	0.046	$4 \cdot 10^{-4}$	0	0.044	$5 \cdot 10^{-6}$	1			
4	0.025	0.027	0.002	1	0.027	$1.5 \cdot 10^{-4}$	0	0.026	$3 \cdot 10^{-6}$	1	0.026	$< 10^{-6}$	0

see that for the problem under consideration the  $(2N + 1)$ -fold angular momentum degeneracy, that is characteristic for the Coulomb problem, is lifted, though two-fold degeneracy of the states with  $\pm l$  remains (at  $l \neq 0$ ). For any  $l$ , we obtain  $\bar{\epsilon}_{l,N} > |\bar{\epsilon}_{N,\text{Coul}}|$ . This is due to the fact that the function  $|\bar{\epsilon}(q)|$  is always less than the kinetic energy for the Coulomb case,  $q^2/2$ . When  $l, N$  increase, the found energies  $\bar{\epsilon}_{l,N}$  become closer to the Coulomb analogs. This can be understood since with increase in  $l, N$ , the wavevectors actual for formation of the quasi-coupled states become smaller, and the difference between functions  $|\bar{\epsilon}(q)|$  and  $q^2/2$  diminishes.

For given  $l, N$ , the obtained coefficients  $\{B_N^l\}$  allow us to calculate the radial wavefunctions,  $R_{l,N}(q)$ , and the total wavefunctions in the momentum space

$$\Phi_{l,N}(\mathbf{q}) = \frac{1}{\sqrt{2\pi}} e^{-i l \phi_q} R_{l,N}(q), \quad (41)$$

with  $q$  and  $\phi_q$  being the polar coordinates of the vector  $\mathbf{q}$ .

Probability to find the electron pair in the  $\{l, N\}$ -bi-electron state with the radial wavevector from the interval  $q, q + dq$  is  $|R_{l,N}(q)|^2 q dq$ . The corresponding probability density in series (37) is presented in Fig. 4a for several long-living bi-electron states (see below the estimates for the decay time of these states). One can see that indeed the bi-electron wavefunctions are concentrated within the region of small  $q$ , where the effective mass of the single-electron spectrum is essentially negative. The larger quantum numbers  $\{l, N\}$ , the smaller actual  $q$ . We found the average values of  $q$  for different  $l, N$ -states:  $\bar{q}_{1,1} = 0.65$ ,  $\bar{q}_{2,2} = 0.3$ ,  $\bar{q}_{3,3} = 0.29$ ,  $\bar{q}_{4,4} = 0.22$ .

The inverse Fourier–Hankel transformation gives the radial wavefunctions in real space,  $R_{l,N}(\rho)$ . We used these functions to calculate the probability to find two electrons within the interval  $\rho, \rho + d\rho$ , i.e.,  $|R_{l,N}(\rho)|^2 \rho d\rho$ . Examples of corresponding probability densities are shown in Fig. 4b. It is seen that the probability densities are extended over large relative distances,  $\rho$ . The average distances between the electrons in different  $\{l, N\}$ -states are:  $\bar{\rho}_{1,1} = 2.7$ ,  $\bar{\rho}_{2,2} = 6.5$ ,  $\bar{\rho}_{3,23} = 12.7$ ,  $\bar{\rho}_{4,4} = 22.5$ , etc.

### 3.3. Decay time calculations

As stressed above, the found  $\{l, N\}$ -bi-electron states have to be quasi-stationary. They decay to free particle states of the same energy. A formal approach to decay time calculations can be found elsewhere [25].

According to this approach, to determine decay of the found states we shall correct their energies and wavefunctions. For example, in the coordinate representation we may use corrected wavefunctions in the form

$$\Psi_{l,N}(\rho) = A_0 R_{l,N}(\rho) + \int d\bar{\epsilon} A_{\bar{\epsilon}} \mathcal{R}_{l,\bar{\epsilon}}(\rho), \quad (42)$$

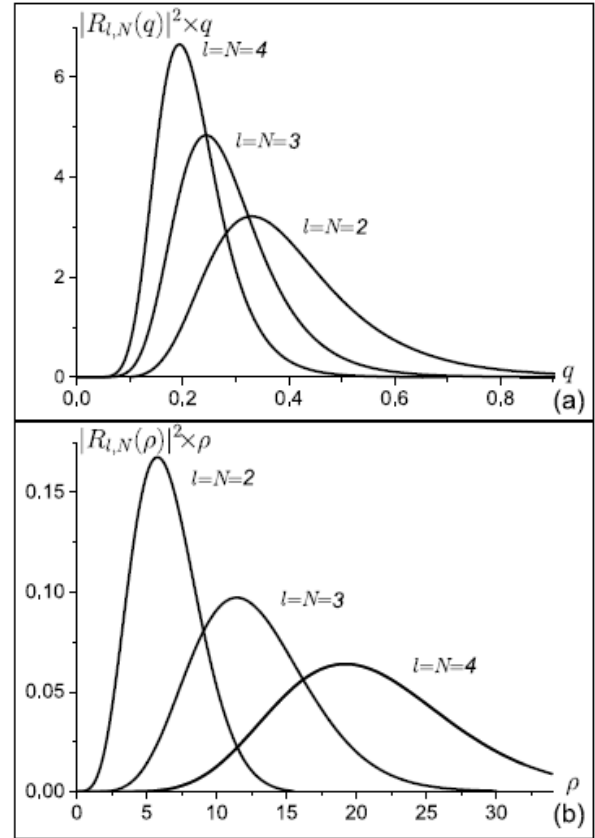


**Fig. 4.** (a) Probability densities to find two electrons with the relative momentum  $q$ . (b) Probability densities to find two electrons at the relative distance  $\rho$ . Results are shown for long living  $\{l, N\}$  bi-electron states.

where  $\mathcal{R}_{l,E}(\rho)$  is the radial functions of free particles given by Eq. (32),  $A_0, A_{\bar{\epsilon}}$  are unknown coefficient and function. Then, applying the perturbation method to initial Eq. (30) we find these coefficients and an imaginary correction to the energy,  $\gamma_{l,N}$ :

$$\bar{\epsilon} \approx \bar{\epsilon}_{l,N} + i\gamma_{l,N}, \quad \gamma_{l,N} = \frac{q_{l,N} |M_{l,N}(q_{l,N})|^2}{|d\bar{\epsilon}(q)/dq|_{q_{l,N}}}, \quad (43)$$

where  $q_{l,N}$  is defined by relationship  $\bar{\epsilon}(q_{l,N}) = \bar{\epsilon}_{l,N}$ , and the matrix element is defined as follows

$$M_{l,N}(q) = \int_0^\infty d\rho J_l(q_n \rho) R_{l,N}(\rho) = \int_0^\infty dq' q' R_{l,N}(q') Q_l(q', q).$$

The calculated values of  $\gamma_{l,N}$  are presented in Table.

The decay factor  $\gamma_{l,N}$  defines broadening and the lifetime of the two-electron coupled states,

$$\tau_{l,N}^{dec} = \frac{\hbar}{2\gamma_{l,N} E_B}.$$

The results obtained for  $\gamma_{l,N}$  are valid if  $\gamma_{l,N} \ll \bar{\epsilon}_{l,N}$ , when the energy level  $\bar{\epsilon}_{l,N}$  is well defined.

Note, for  $l = N = 0$  we obtained  $\gamma_{l,N} \gg \epsilon_{l,N}$ , which can be interpreted as the *nonexistence* of such a state. For  $l \geq 1$ , we obtain  $\gamma_{l,N}/\epsilon_{l,N} < 1$ . This ratio rapidly decreases with increase in  $l$ . For  $l, N \geq 3$ , we find that  $\gamma_{l,N}/\epsilon_{l,N} < 10^{-4}$ . This correlates with conclusions of the semiclassical analysis made in Subsection 2.3 for the same parameters: semi-classical closed trajectories arise at  $l \geq 3$ . In addition, for finite values of the angular momenta calculated energies,  $\epsilon_{l,N}$ , belong to the same energy intervals, for which the closed trajectories in the phase-plane are predicted.

### 3.4. Spin states of coupled electrons

Consider briefly spin states of the coupled electron pair. We neglect interaction between spins and orbital motion, which allows us to present the total wavefunction of two electrons as a product of orbital and spin wavefunctions:

$$\Psi(\mathbf{r}_1, \sigma_1, \mathbf{r}_2, \sigma_2) = \Psi(\mathbf{r}_1, \mathbf{r}_2)S(\sigma_1, \sigma_2),$$

where  $\sigma_1, \sigma_2$  are the electron spins and  $S(\sigma_1, \sigma_2)$  is a spin function. The Pauli exclusion principle states that for two identical fermions the total wave function is anti-symmetric with respect to exchange of the particles. It is easy to find symmetry properties of the orbital wavefunction of Eq. (28) with respect to permutation  $\mathbf{r}_1 \rightarrow \mathbf{r}_2$ . Indeed, this permutation corresponds to changing  $\mathbf{r} \rightarrow -\mathbf{r}$  or, in the polar coordinates,  $\{\rho, \phi\}$ , to substitution  $\phi \rightarrow \phi + \pi$ . The latter means that for the states with even angular momentum  $l$  the orbital wavefunction is symmetric, while those are anti-symmetric for odd  $l$ . Thus, to satisfy the Pauli exclusion principle for even  $l$ , the spin function should be anti-symmetric, which corresponds to total spin  $\Sigma$  of the electron pair equals 0. For odd  $l$ , the spin function should be symmetric, which implies that the total spin of the pair equals 1.

### 3.5. Moving bi-electron

So far, we considered that the center-of-mass of the electron pair is motionless, which is valid when the total momentum of the pair,  $\mathbf{P}$ , is zero. If  $\mathbf{P} \neq 0$ , the electron pair is moving as a whole. For the nonparabolic energy dispersion,  $\epsilon(\mathbf{p})$ , this translational motion and relative motion of the electrons in the pair cannot be separated. However, assuming that  $\mathbf{P}$  is small, we can estimate the kinetic energy of the pair and its effective mass. In so doing, we use the expansion of the Hamiltonian (1) in series with respect to  $\mathbf{P}$ :

$$\begin{aligned} H &\approx H_0(\mathbf{p}, \mathbf{r}) + \frac{1}{4p} \frac{d\epsilon}{dp} \mathbf{P}^2 + \frac{1}{4p^2} \left[ \frac{d^2\epsilon}{dp^2} - \frac{1}{p} \frac{d\epsilon}{dp} \right] (\mathbf{Pp})^2 \equiv \\ &\equiv H_0(\mathbf{p}, \mathbf{r}) + \delta H(\mathbf{p}, \mathbf{P}), \end{aligned} \quad (44)$$

where  $d\epsilon/dp$  and  $d^2\epsilon/dp^2$  are functions of magnitude of the relative momentum  $\mathbf{p}$ ;  $\delta H(\mathbf{p}, \mathbf{P})$  is a correction to the Hamiltonian  $H_0$  caused by motion of the center-of-mass. Using the scaling of Eqs (20), we rewrite this correction as

$$\delta \mathcal{H}(\mathbf{k}, \mathbf{Q}) = \frac{\delta H}{E_B} = \frac{1}{8k} \frac{d\epsilon}{dk} \mathbf{Q}^2 + \frac{1}{8k^2} \left[ \frac{d^2\epsilon}{dk^2} - \frac{1}{k} \frac{d\epsilon}{dk} \right] (\mathbf{Qk})^2,$$

with  $\mathbf{Q} = \mathbf{P}/p_B$ . Applying the perturbation theory method [26] for the  $\{l, N\}$ -state of bi-electron, we obtain the energy correction in the form:

$$\delta \epsilon_{l,N}(\mathbf{Q}) = \frac{\mathbf{Q}^2}{2\mathfrak{M}_{l,N}}, \quad \frac{1}{\mathfrak{M}_{l,N}} = \frac{1}{8} \int_0^\infty dq |R_{l,N}(q)|^2 \left[ \frac{d\epsilon}{dq} + q \frac{d^2\epsilon}{dq^2} \right]$$

where  $\delta \epsilon_{l,N}(\mathbf{Q})$  and  $\mathfrak{M}_{l,N}$  can be interpreted as the dimensionless kinetic energy and the *effective mass* of the bi-electron in the  $\{l, N\}$ -state. Dependence of the effective mass of the bi-electron on its “internal” state is, obviously, manifestation of interaction of center-of-mass motion and internal relative motion.

Note, the wavefunctions  $R_{l,N}(q)$  are mainly localized in the range of small  $q$ , where both terms in Eq.

$$(45), \quad \frac{d\epsilon}{dq} \quad \text{and} \quad \frac{d^2\epsilon}{dq^2},$$

are negative. This implies that the effective mass of the bi-electron should be also negative.

For the discussed example of bigraphene on the SiO<sub>2</sub> substrate, the dimensionless effective masses of the bi-electron in different  $\{l, N\}$ -states are:  $\mathfrak{M}_{1,1} = -16.6$ ,  $\mathfrak{M}_{2,2} = -6$ ,  $\mathfrak{M}_{3,3} = -4.8$ ,  $\mathfrak{M}_{4,4} = -4.47$ . Note, for scaling (20), the dimensionless mass of two non-interacting electrons with  $q \rightarrow 0$  equals  $-4$ . Thus bi-electrons are “heavy” particles with negative masses.

## 4. Discussion

In this paper, we have analyzed interaction of two electrons from the same energy band with the complex single-particle energy dispersion. Both semiclassical and quantum considerations have shown that two electrons with the MH single-electron energy dispersion,  $\epsilon(\mathbf{p})$ , can form a composite quasi-particle – the bi-electron. The coupling energies – energy of relative motion of the two electrons – are positive (with respect to  $2\epsilon(0)$ ). That is, the bi-electron corresponds to an excited state of the electron system. Bi-electron coupled states exist in the continuum of extended (free) states inherent to the electron pair. Thus, according to the quantum mechanics, the found two-electron coupled states are of quasi-resonant character and have finite times of life. Their times of life increase with the increase of angular momentum, thus more stable are the rotating bi-electrons. The semiclassical analysis also leads to stable coupled electron pair only at finite values of the angular momentum. Besides, the semiclassical analysis showed that relative motion of two electrons has a peculiar character: depending on the energy and the angular momentum (*i.e.*, on the impact parameter), e-e scattering can have three reversal points and reversal points at non-zero radial momentum, *etc.*

The coupling energy, lifetime, angular momentum, radius and other characteristics of the bi-electrons are defined by the particular  $\epsilon(\mathbf{p})$ -dependence and dielectric properties of the system. Let us discuss these parameters

for the above considered example of bigraphene on the SiO<sub>2</sub> substrate in the transverse electric field. Using the scaling given in Eqs (24), for relatively stable bi-electron states one can find:  $E_{2,2} = 12.4$  meV,  $\tau_{2,2}^{dec} = 0.5$  ps,  $\bar{r}_{2,2} \approx 29.8$  nm;  $E_{3,3} = 5.6$  meV,  $\tau_{3,3}^{dec} = 1$  ns,  $\bar{r}_{3,3} \approx 58.2$  nm;  $E_{4,4} = 3.3$  meV,  $\tau_{4,4}^{dec} > 5$  ns,  $\bar{r}_{4,4} \approx 100$  nm, where  $E_{l,N}$ ,  $\tau_{l,N}^{dec}$  and  $\bar{r}_{l,N}$  are the bi-electron energy, lifetime and radius in the  $\{l, N\}$ -state, respectively. As seen, the quasi-coupled states with large angular momenta ( $l \gg 3$ ) have macroscopically long lifetimes. Note, just these coupled bi-electron states are allowed in the semiclassical theory. The sizes (radii) of these states are also large ( $\bar{r} > 50$  nm), they increase  $\propto N$  at  $N \gg 1$ .

Note also, for the parameters discussed above the distances to the upper valence band and the first excited electron band are estimated to be 0.21 eV and 0.31 eV, respectively, which are much larger than the found coupling energies of the bi-electron, 0.012...0.003 eV. That proves applicability of the single band approximation used in this paper.

For the same bigraphene, varying the transverse electric field and/or dielectric environment, one can change parameters of the bi-electrons. As an example, consider briefly the free-standing bigraphene, when one can set  $\kappa_0 = 1$ . Then, according to the scaling (24) at the voltage bias of the same amplitude the coupling energies of the bi-electrons should be larger than those discussed above by factor  $(1 + \kappa_{0, \text{SiO}_2})^2/4 \approx 6$  and the corresponding radii of the quantum states should be smaller by factor  $\approx 2.5$ .

The bi-electron can move as a whole. This translational motion can be characterized by the total momentum of the composite particle. At small values of the total momentum, the kinetic energy of the bi-electron is a quadratic function of the momentum. Thus, one can introduce an effective mass of the bi-electron. Due to strongly nonparabolic character of the energy dispersion, the translational motion is coupled to relative motion of electrons composing the bi-electron. As the result, the effective mass of bi-electron depends on its quantum state. Using the scaling given by Eqs (20) and results of Subsection 3.5, for the analyzed example of bigraphene, we obtain the following values of the effective mass:  $-0.46m_0$  for  $l = N = 1$ ;  $-0.17m_0$  for  $l = N = 2$ ;  $-0.13m_0$  for  $l = N = 3$  and  $-0.12m_0$  for  $l = N = 4$ , while the effective mass of a single electron at  $k = 0$  equals  $-0.056m_0$ . Thus, the effective mass of the bi-electron is negative and considerably varies with quantum numbers,  $l, N$ .

Above, properties of the bi-electron were illustrated for the example of bigraphene in transverse electric field. For this case, the MH single-electron energy spectrum is induced by an external voltage. For realistic voltages, critical parameters of the MH spectrum ( $p_m, \epsilon(p_m), M$ ) are such that energies of coupled states are relatively small ( $\leq 10$  meV) and radii of states are large ( $\geq 50$  nm). For two-dimensional crystals with intrinsic MH spectrum (for example, III-VI compounds [5, 6]), the characteristic parameters are favorable for formation of the bi- particles with larger coupling energies and stronger localization.

## 5. Summary

We analyzed interaction of a pair of electrons, which are characterized by the mexican-hat single-electron energy dispersion. We have showed that relative motion of the electron pair is of a very peculiar character. For example, the real space trajectories corresponding to electron-electron scattering can have three reversal points and reversal points at non-zero radial momentum. These trajectories are strongly different from the usual ones. Despite the repulsive Coulomb interaction, two electrons can be coupled forming a composite particle – the bi-electron. The bi-electron corresponds to excited states of two-electron system. The bi-electron coupled states exist in continuum of extended (free) states inherent to the electron pair. Thus, the found bi-electron states are of quasi-resonant character and have finite lifetimes. We found that the rotating bi-electron is the long-living composite particle. When spin-orbital interaction is negligibly small, the bi-electron states with even angular momenta have zero spin (singlet states), while those with odd angular momenta have unitary spin (triplet states). The bi-electrons can be in translational motion. For a slowly moving bi-electron, we have determined the kinetic energy and the effective mass of the composite particle. Due to the strongly nonparabolic energy dispersion, translational motion of the bi-electron is coupled to its internal motion. This results in effective masses depending on the quantum states of bi-electron.

The studied rotating bi-electron replenishes the list of composite quasi-particles with the Coulomb interaction, which are already known for low-dimensional structures, such as excitons, negatively and positively charged excitons (trions) [27–29], and more complex fractionally-charged quasi-particles (anyons) under the fractional Hall effect [30], *etc.* Because there is a number of indications that the mexican-hat single-electron energy dispersion occurs for novel two-dimensional materials, we have suggested that investigation of rotating bi-electrons may bring new interesting effects in low-dimensional and low-temperature physics.

## References

1. Castro Neto A.H., Guinea F., Peres N.M.R., Novoselov K.S., and Geim A.K. The electronic properties of graphene. *Rev. Mod. Phys.* 2009. **81**, No 1. P. 109–163. <https://doi.org/10.1103/RevModPhys.81.109>.
2. Orlita M. and Potemski M. Dirac electronic states in graphene systems: optical spectroscopy studies. *Semicond. Sci. Technol.* 2010. **25**. P. 063001. <https://doi.org/10.1088/0268-1242/25/6/063001>.
3. Zolyomi V., Drummond N.D., Falko V.I. Band structure and optical transitions in atomic layers of hexagonal gallium chalcogenides. *Phys. Rev. B.* 2013. **87**. P. 195403. <https://doi.org/10.1103/PhysRevB.87.195403>.

4. Rybkovskiy D.V., Osadchy A.V., Obraztsova E.D. Transition from parabolic to ring-shaped valence band maximum in few-layer GaS, GaSe, and InSe. *Phys. Rev. B*. 2014. **90**. P. 235302. <https://doi.org/10.1103/PhysRevB.90.235302>.
5. Wickramaratne D., Zahid F., Lake R.K. Electronic and thermoelectric properties of van der Waals materials with ring-shaped valence bands. *J. Appl. Phys.* 2015. **118**. P. 075101. <https://doi.org/10.1063/1.4928559>.
6. Kibirev I.A., Matetskiy A.V., Zotov A.V., and Saranin A.A. Thickness-dependent transition of the valence band shape from parabolic to Mexican-hat-like in the MBE grown InSe ultrathin films. *Appl. Phys. Lett.* 2018. **112**. P. 191602. <https://doi.org/10.1063/1.5027023>.
7. Ortner K., Zhang X.C., Pfeuffer-Jeschke A., Becker C.R., Landwehr G. and Molenkamp L.W. Valence band structure of HgTe/Hg<sub>1-x</sub>Cd<sub>x</sub>Te single quantum wells. *Phys. Rev. B*. 2002. **66**. P. 075322. <https://doi.org/10.1103/PhysRevB.66.075322>.
8. Minkov G.M., Germanenko A.V., Rut O.E., Sherstobitov A.A., Dvoretzki S.A., and Mikhailov N.N. Weak antilocalization in HgTe quantum wells with inverted energy spectra. *Phys. Rev. B*. 2012. **85**. P. 235312. <https://doi.org/10.1103/PhysRevB.85.235312>.
9. Jiang Y., Thapa S., Sanders G.D. *et al.* Probing the semiconductor to semimetal transition in InAs/GaSb double quantum wells by magneto-infrared spectroscopy. *Phys. Rev. B*. 2017. **95**. P. 045116. <https://doi.org/10.1103/PhysRevB.95.045116>.
10. Gross E.F., Perel V.I., Shekhmametev R.I. Inverse hydrogenlike series in optical excitation of light charged particles in a bismuth iodide (BiI<sub>3</sub>) crystal. *JETP Lett.* 1971. **13**. P. 229.
11. Rashba E.I., Edelstein V.M. Magnetic Coulomb levels near the saddle points. *JETP Lett.* 1969. **9**. P. 287–290.
12. Mahmoodian M.M., Chaplik A.V. Bielectron formed in a 2D system by the spin orbit interaction and image forces. *JETP Lett.* 2018. **107**. P. 564–568. <https://doi.org/10.1134/S0021364018090084>.
13. Sabio J., Sols F., and Guinea F. Two-body problem in graphene. *Phys. Rev. B*. 2010. **81**. P. 045428. <https://doi.org/10.1103/PhysRevB.81.045428>.
14. Lee R.N., Milstein A.I., and Terekhov I.S. Quasi-localized states in a model of electron-electron interaction in graphene. *Phys. Rev. B*. 2012. **86**. P. 035425. <https://doi.org/10.1103/PhysRevB.86.035425>.
15. Marnham L.L. and Shytov A.V. Metastable electron-electron states in double-layer graphene structures. *Phys. Rev. B*. 2015. **92**. P. 085409. <https://doi.org/10.1103/PhysRevB.92.085409>.
16. Sablikov V.A. Two-body problem for two-dimensional electrons in the Berner-Hughes-Zhang model. *Phys. Rev. B*. 2017. **95**. P. 085417. <https://doi.org/10.1103/PhysRevB.95.085417>.
17. Downing C.A., Portnoi M.E. Bielectron vortices in two-dimensional Dirac semimetals. *Nature Commun.* 2017. **8**. Art. No 897. <https://doi.org/10.1038/s41467-017-00949-y>.
18. Kevorkian J. and Cole J.D. *Perturbation Methods in Applied Mathematics*. Springer-Verlag, New York, 1998.
19. By simple substitutions  $r \rightarrow rp\phi$ ,  $t \rightarrow tp\phi$  one can show that for a given energy dispersion  $\epsilon(p)$ , the only actual parameter in Eqs (4), (5) and (9) that has an effect on trajectories in the phase-plane, as well as in real space,
20. Landau L.D. and Lifschitz E.M. *Mechanics*. Pergamon Press, Oxford, 3rd edition, 1976.
21. The single energy band equation can be used for the analysis of electron states with energies nearby this band, when contributions of other remote energy bands are negligible.
22. Gradshteyn I.S. and Ryzhik I.M. *Table of Integrals, Series, and Products*. 6th edition. Academic Press, San Diego, 2000.
23. Bronshtein I.N., Semendyayev K.A., Musio G. and Muehlig H. *Handbook of Mathematics*. Springer-Verlag, New York, 4th edition, 2004.
24. Shibuya T. and Wulfman C.E. The Kepler problem in two-dimensional momentum space. *Am. J. Phys.* 1965. **33**. P. 570. <https://doi.org/10.1119/1.1971931>.
25. Parfitt D.G.W. and Portnoi M.E. The two-dimensional hydrogen atom revisited. *J. Math. Phys.* 2002. **43**. P. 4681. <https://doi.org/10.1063/1.1503868>.
26. Vasko F.T., Raichev O.E. *Quantum Kinetic Theory and Applications. Electrons, Photons, Phonons*. Kluwer Academic Publisher, Boston, 2005.
27. L.D. Landau and E.M. Lifshitz, *Quantum Mechanics (Non-relativistic Theory)*. Pergamon Press, Oxford, 3rd edition, 1977.
28. Lampert M.A. Mobile and immobile effective-mass-particle complexes in nonmetallic solids. *Phys. Rev. Lett.* 1958. **1**. P. 450. <https://doi.org/10.1103/PhysRevLett.1.450>.
29. Kheng K., Cox R.T., d'Aubigné M.Y., Bassani F., Saminadayar K., and Tatarenko S. Observation of negatively charged excitons  $X^-$  in semiconductor quantum wells. *Phys. Rev. Lett.* 1993. **71**. P. 1752. <https://doi.org/10.1103/PhysRevLett.71.1752>.
30. Shields A.J., Osborne J.L., Simmons M.Y., Pepper M., and Ritchie D.A. Magneto-optical spectroscopy of positively charged excitons in GaAs quantum wells. *Phys. Rev. B*. 1965. **52**. P. R5523. <https://doi.org/10.1103/physrevb.52.r5523>.
31. Prange R.E. and Girvin S.M. *The Quantum Hall Effect*. Springer-Verlag, New York, 1987; Chakraborty T. and Pietilainen P. *The Quantum Hall Effects: Integer and Fractional*. Springer, Berlin, 2nd edition, 1995.

## Author and CV



**Viacheslav Kochelap**, Prof., Corresponding Member of NAS of Ukraine, Head of the Department of Theoretical Physics at the V. Lashkaryov Institute of Semiconductor Physics, NAS of Ukraine. He was born in 1944 in Kyiv (Ukraine), graduated in theoretical physics in 1966 from the Kyiv State University, received the PhD degree in theoretical physics in 1970 from the Institute of Semiconductor Physics, NAS of Ukraine, the Doctor of Phys.-Math. Sciences (Habilitation degree) in physical electronics & quantum electronics, 1984, full Professor from 1987. V. Kochelap is the author of more than 250 publications. His main research activity is in fields of low-dimensional systems, electron and phonon transports, fluctuation phenomena, THz-physics of semiconductors, as well as semiconductor nanoscale devices. <https://orcid.org/0000-0002-7181-0356>

## Бі-електрон, що обертається, у двовимірних системах з одно-електронною енергією типу мексиканського капелюха

### В.А. Кочелап

**Анотація.** Ряд нових двовимірних матеріалів і наноструктур демонструє складну залежність одно-електронної енергії від імпульсу, яка подібна мексиканському капелюху. У статті проаналізовано взаємодію пари електронів з такою енергетичною дисперсією. Показуємо, що відносний рух електронної пари має дуже своєрідний характер. Наприклад, траєкторії в реальному просторі, які відповідають електрон-електронному розсіюванню, можуть мати три точки розвороту, точки розвороту при ненульовому радіальному імпульсі та інші незвичайні особливості. Незважаючи на відштовхувальну кулонівську взаємодію, два електрони можуть з'єднуватися, утворюючи складну квазічастинку – бі-електрон. Бі-електрон відповідає збудженим станам дво-електронної системи. Оскільки бі-електронні зв'язані стани існують у континуумі вільних станів електронної пари, ці стани є квазі-резонансними та мають скінченний час життя. Виявлено, що бі-електрон, який обертається, є довгоіснуючою складною квазічастинкою. Оберткові бі-електрони можуть перебувати в русі. Для повільного руху бі-електронів визначено кінетичну енергію та ефективну масу. Через сильно непараболічну дисперсію енергії поступальний рух бі-електрона є пов'язаним з його внутрішнім рухом. Це приводить до того, що ефективна маса залежить від квантових станів бі-електрона. У статті властивості бі-електрона проілюстровано на прикладі біграфену, до якого прикладено поперечне електричне поле.

Ми вважаємо, що дослідження оберткових бі-електронів, що утворюються при одно-електронній дисперсії енергії подібної до мексиканського капелюха, можуть виявити нові цікаві ефекти у фізиці двовимірних кристалів при низьких температурах.

**Ключові слова:** бі-електрон, енергетична дисперсія, біграфен.